CHAPTER 2:

BACKGROUND

2.1. Single Crystals: *Structure of Au Surfaces*

For a detailed understanding of surface processes, the use of single-crystal electrodes with structurally well-characterized surfaces is necessary. Polycrystalline surfaces, routinely employed in the early days of electrochemical surface studies, are far too complicated for a reliable interpretation on an atomic level. Single-crystal surfaces need to be prepared and their structure characterized, which is by no means a trivial task for electrochemists.

The surface of a crystalline solid is strongly correlated to its bulk structure. The atoms of a crystal are arranged in a periodical sequence forming the crystal lattice. Most frequently metals and metal alloys tend to form close-packed sphere (cps) arrangements reflecting the isotropy of the forces atomic interaction. There are two possible cps arrangements, the hexagonal close-packed (hcp) and the face centered cubic (fcc) crystal lattice. In both cases the planes of highest atomic density, (0001) and (111), respectively, have the same two-dimensional (2D) structure at the surface.

Gold crystallizes in the face centered cubic lattice (fcc), and through indexing of the different lattice plains and characteristic planes arise within the elementary cell. Miller indices are used as notation to describe lattice planes and directions in a crystal. Some directions and planes have a higher density of nodes; these dense planes have an influence on the behaviour of the crystal. The most important surfaces structures become indicated represented lattice plains through that low (100), (110) as well as (111) (Fig. 2.1).

(100)   (110)   (111)
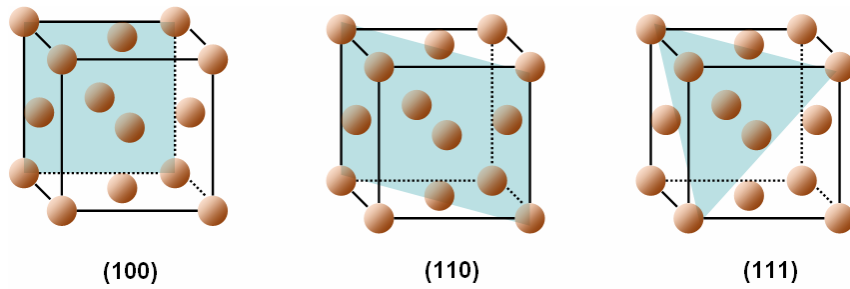
Figure 2.1: *Lattice planes in an fcc cubic structure.*

## 2.2. Structure of Electrified Interfaces

2.2.1. The Double Layer Region

The electrical double layer is described as the variation of electric potential near a surface, and it has a large bearing on the behaviour of colloids and other surfaces in contact with solutions. The earliest model of the electrical double layer is usually attributed to Helmholtz (1879). Helmholtz treated the double layer mathematically as a simple capacitor, based on a physical model in which a single layer of ions is adsorbed at the surface. In this model, it is supposed that the solvated ions range themselves along the surface of the electrode but are held away from it by the molecules in their solvation spheres. The location of the sheet of ionic charge, which is called the *outer Helmholtz plane (OHP)*, is identified as the plane running through the solvated ions. The imaginary plane crossing the radius of the specific adsorbed ions is termed *inner Helmholtz plane (IHP)*. The Helmholtz model ignores the disrupting effect of thermal motion, which tends to break up and disperse the rigid wall of charge. Important approximations used in this model are:

- Ion are effectively point charges
- The only significant interactions are coulombic
- Electrical permittivity is constant throughout the double layer
- The solvent is uniform at the atomic scale.

Later Gouy and Chapman (1910-1913) made significant improvements by introducing a diffuse model of the electrical double layer, in which the potential at a surface decreases

exponentially due to adsorbed counter-ions from the solution. In this model, the disordering effect of the thermal motion is taken into account.
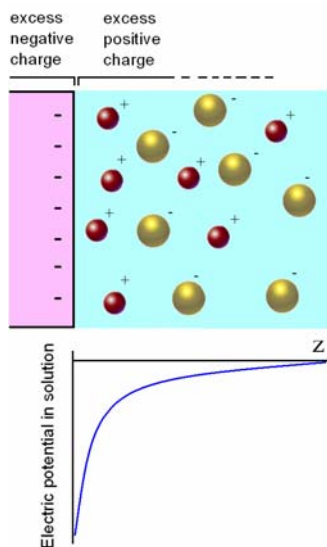
Figure 2.2: *The Gouy-Chapman model of the electric double layer*.

Local concentrations of cations and anions differ in the Gouy-Chapman model from their bulk concentrations (Fig. 2.2). The modification of the local concentrations near an electrode implies that it might be misleading to use activity coefficients characteristic of the bulk to discuss the thermodynamic properties of ions near to the interface. This is one the reasons why measurements in dynamic electrochemistry are almost always done using a large excess of supporting electrolyte (e.g. a 1 M solution of a salt, an acid, or a base). Under such conditions the activity coefficients are almost constant because the inert ions dominate the effects of local changes caused by any reactions taking place.

The Gouy-Chapman-Stern model combines the Helmholtz single adsorbed layer model with the Gouy-Chapman diffuse layer model. The ions closest to the electrode are constrained into a rigid Helmholtz plane while outside that plane the ions are dispersed like in the Gouy-Chapman model. Fig. 2.3 demonstrates the representation of this model.
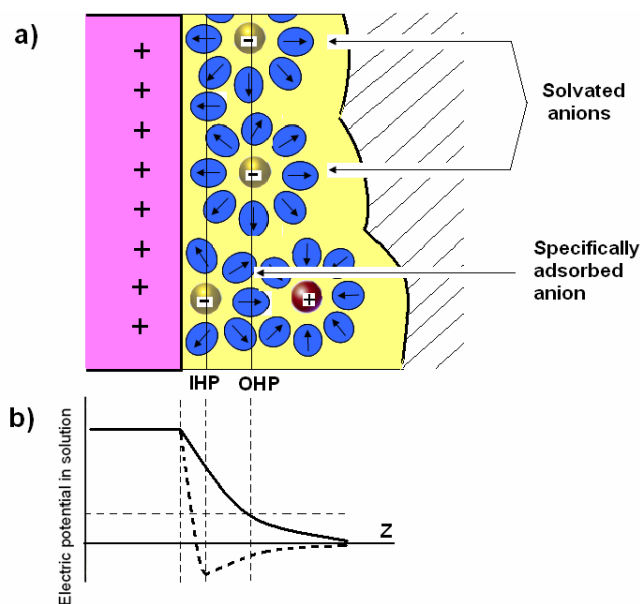
Figure 2.3 a: *The Gouy-Chapman-Stern model of the electric double layer.* ***b:*** *Potential distribution across the electrochemical interface for a purely electrostatic intercation between solvated ions and the metalic surface (solid curve) and for the case of specifically adsorbing anions (dashed curve).*

The solvated ions at the OHP which interact with the electrode surface by electrostatic forces only, are considered as *nonspecifically adsorbed*. These are ions with strongly bound solvation shells such as most cations or F^-. Other ions, mostly anions like Cl^-, Br^- or I^- with relatively weakly bound solvation shells, may partly strip their solvation shell in the double layer and undergo a direct chemical bond (covalent and ionic) with the electrode surface. Such chemisorbed ions are called *specifically* adsorbed and their location defines the so-called inner Helmholtz plane (IHP). While the surface concentration of a nonspecifically adsorbed ion hardly exceeds 0.1 - 0.2 of a full monolayer to establish (maximum) potential drops of about 1 V, the coverage of specifically adsorbed ions can be much higher (up to close packing); however, their ionic character is then strongly reduced. In addition, the lateral arrangement and hence, the coverage of specifically adsorbed ions depends markedly on the substrate structure and varies significantly between different crystallographic orientations. The tendency of an ion to adsorb specifically (to chemisorb on the electrode surface) depends on the balance between its chemical interaction with the substrate and the heat of solvation. For anions on Ag or Au single-crystal surfaces the following sequence for the tendency of chemisorption has been established: $F^- \approx$

$ClO_4^- < SO_4^{2-} < Cl^- < Br^- < I^-$. Even anions like F^- and ClO_4^- show a slight tendency towards specific adsorption, as will be demonstrated in relation to surface reconstruction later [61].

2.2.2. Potential of Zero Charge (PZC)

Potential of zero charge (PZC) is a fundamental electrochemical characteristic of metal, plays a major role in electrocapillary and electrokinetic phenomena, electrical double-layer structure, adsorption of ions and neutral organic molecules on electrode. The PZC is commonly defined as the potential at which the electrode surface has no excess charge, and a number of techniques have been developed for its determination. In the case of liquid electrodes such as Hg or Ga, the PZC can be derived directly from the maximum of the corresponding electrocapillary curve [38]. For noble metals such as Ag or Au with a sufficiently broad double layer charging region, the PZC can be obtained from measurements of the double layer capacitance in dilute solutions, where it manifests itself by a pronounced minimum in the double layer capacity [62]. This technique, however, cannot be employed for the more reactive metals, such as transition metals, where the formation of adlayers or surface oxides occurs over a wide potential range.

Differential capacity minimum technique is one of the experimental methods of determination of the PZC. The background of this technique can be explained as follows: It is well known that [38]

$$\frac{1}{C_{double\,layer}} = \frac{1}{C_{Helmholtz}} + \frac{1}{C_{diffuse}} \qquad \text{(Eq. 2.1)}$$

In dilute solution (c<0.05 M), $C_{diffuse}$ is sufficiently small so that it significantly affects the double-layer capacitance. $C_{diffuse}$ is also reduced, that is, its influence increased, as $q_{diffuse}$ approaches zero and hence dominating part of the capacitance around the pzc when C_{DL} is almost entirely $C_{diffuse}$. Determination of the dip to a sharp minimum in the C_{DL}-V curve therefore identifies the potential for q_m=0.

This method for determination of pzc was proposed by Vorsina and Frumkin [63]. For it to be applicable, the measured C must be that of the double layer and not have important components due to the pseudocapacitance effects. This condition is indicated by the frequency independence of the capacitance. Absence of chemisorption leads to the necessary constancy of

$C_{Helmhotz}$ with concentration and is indicated by a plot of $1/C_{DL}$ against $1/C_{diffuse}$ with a slope of the unity (Parsons-Zobel criterion).

PZC value can be influenced by the adsorption of ions. Weak specific adsorption of ions does not lead to a significant PZC shift. However, strong specific anion adsorption shifts the PZC in the negative direction in the range of ~100-200 mV; the shift increases with rising surface activity of anions in the sequence $F^- < Cl^- < Br^- < I^-$.
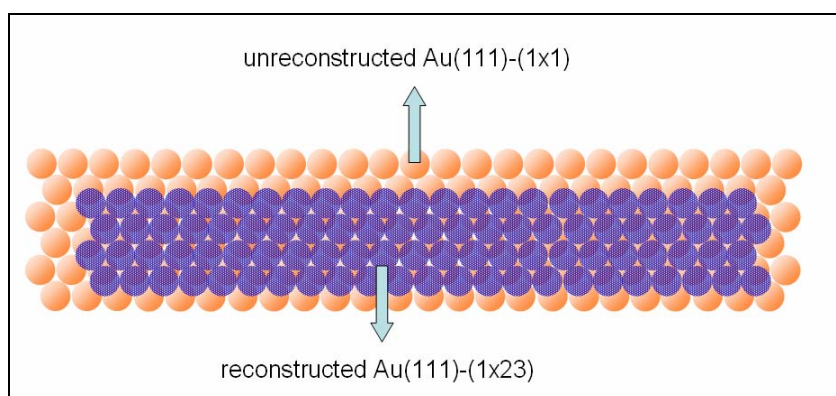
2.2.3. Surface Reconstruction

Surface atoms of solids are often found at positions that clearly differ from those expected for an ideal termination of the bulk. This deviation is the result of imbalanced forces at the surface at which atoms are located asymetrically compared to the atoms in the bulk. In a number of cases surface atoms undergo a lateral displacement to form markedly different surface structures. Such a rearrangement of the surface atoms' positions, which is driven by a lowering of the surface energy, is called *surface reconstruction*. A driving force for surface reconstruction is considered to be a surface stress [64].Heine and Marks [65, 66] pointed out that an increase of surface electron density gives a contarctive surface stress. This phenomenon is observed under UHV as well as under in-situ electrochemical conditions. Surface reconstruction can be induced either thermally or by the electrode potential.

It has been well known that the low index surfaces of Au undergo reconstruction in vacuum [67]. On the other hand, Hamelin [68], Kolb and Schneider [61, 69] found that reconstruction also occurs on the surface of Au(100), Au(110) and Au(111) electrodes in solution at negative electrode potentials, and is lifted when the electrode potential become more positive. Surface stress of electrode was found to be a function of electrode potential and the electrode surface charge.

The reconstruction of Au(111) has been studied by several groups [61, 69-71]. The reconstructed surface has a 4 % higher atom density than the unreconstructed surface. As result of reconstruction of Au(111), a (1x23) surface is formed, causing every 23rd atom to be registered with the underlying bulk atoms (Fig. 2.4). The reconstructed surface has a characteristic stripe-like appearance. When the surface is positively charged, the reconstruction is lifted and the gold atoms relax back into the positions on the truncated 3-D lattice, to form a hexagonal structure.

Adsorbed anions have a significant impact on the crystlallography of the Au(111) electrode, causes the removal of reconstructed surface. During the lifting of the reconstruction, the excess 4 % reconstructed atoms are expelled resulting in a degree of roughness which might alter the electrochemical behaviour of the electrode. The structural change from reconstructed (1x23) to an unreconstructed (1x1) surface takes place around the PZC at which the concentration of anions starts to accelerate at the surface. In general, the adsorption of anions (particularly halides) assists in lifting the reconstruction of the Au(111) surface [65, 66].

Figure 2.4: *The reconstructed Au(111).*

2.3 Adsorption of Organic Molecules on the Electrode Surface

It is well known that neutral organic molecules such as the DNA bases adsorb on mercury and on single crystal electrodes. The adsorbates undergo two-dimensional, first order phase-transition forming well-ordered films if critical conditions (temperature, concentration and potential) are reached [20-22, 25, 26]. Below that conditions the molecules are randomly oriented forming a two-dimensional gas-like phase. The phase-transition of the adsorbate takes place by a nucleation and growth process. The formation of the condensed film by 2-D nucleation and growth represent a first order phase transition in which an expanded phase is transformed in a condensed one by discontinuous change of the relative surface concentration. To form a condensed film, the single molecules must first aggregate to small clusters of a certain minimum size called "critical nuclei" before expand in a new phase. As soon as the cluster formed reaches the critical size, it can expand by incorporating additional molecules and form the condensed film.

Adsorption phenomena including 2D phase transitions at electrochemical interfaces may be classified, according to the binding energy of the adsorbate onto the surface, in two categories. *Physisorption* corresponds to small binding energies, the substrate–adsorbate interactions are mainly due to van der Waals forces and involve almost no mixing between the orbitals of the adsorbate and the substrate [72]. Lateral interactions between the adsorbed species are dominated by dipole–dipole, dipole–induced dipole and hydrophobic interactions, π-stacking and/or hydrogen bonding [73].

Chemisorption represents the formation of a surface chemical bond, which is either covalent (sharing of electrons) or ionic (electron transfer). The understanding of chemisorption phenomena is rather complex and requires knowledge on the geometrical structure of the system, adsorbate binding and charge transfer, the electronic structure of adsorbate and substrate as well as vibrational frequencies [73].

The mercury electrode is the most recommended electrode to study the kinetic of the film formation due to the low RC constant and the well defined surface; however, working with solid single crystal electrode allows investigating the structure of physisorbed and chemisorbed condensed films by STM and some *ex-situ* experiments.

2.4 Metal Underpotential Deposition (Me UPD)

Underpotential deposition (UPD) is an electrochemical phenomenon in which only a full monolayer or a submonolayer of a foreign metal is deposited on the electrode at potentials positive of the reversible Nernst potentials. Because of the work function difference between the adatom and the substrate, the formation of the adatom-substrate bond occurs prior to that of adatom-adatom bond during bulk deposition. The monolayer formed during the UPD process is interesting not only due to their physical properties which are different from bulk phases of either the surface or the adatom, but also because they exhibit catalytic activity toward the electrooxidation of small organic molecules [74, 75].

Underpotentially deposited metal monolayers have attracted considerable interest because they appear to be ideal systems for developing a basic understanding of adatom-substrate, adatom-adatom and adatom-superstrate (solvent or adion) interactions. They provide easily accessible, stable adlayers and the shapes of voltammograms, adsorbtion peak potentials,

coverages, charge transfer kinetics are very sensitive to the substrate crystallographic orientation and to the composition of the electrolyte.

Fig. 2.5 depicts the constituent processes involved in the monolayer formation of metal (M) on a substrate (S) in the double layer region. Two processes take place during the monolayer formation of M on S, which can be envisaged as follows:

(i)   movement of the solvated ions from the bulk to the reaction zone, getting rid of their solvation sheath, and

(ii)   electron transfer from the substrate to the metal ions leading to the subsequent bond formation with the substrate (S). The S–M bond formation involving the defective sites occurs after knocking off the adsorbed solvent dipoles from the appropriate sites of the substrate
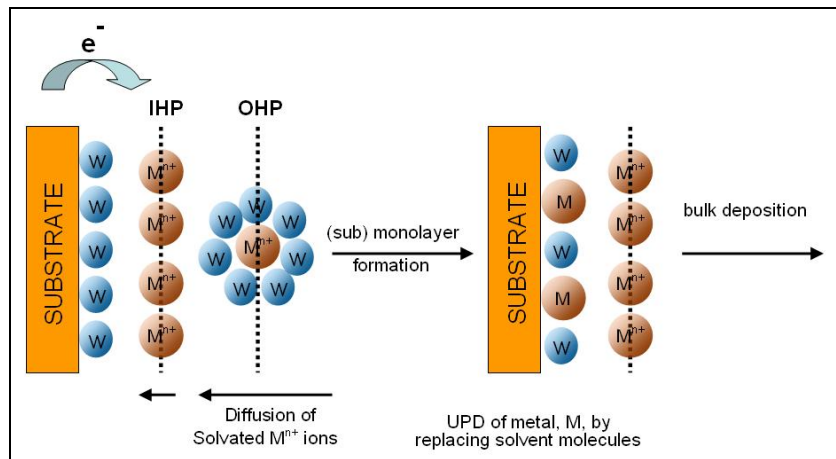
Figure 2.5: *Schematic description of processes constituting adsorption of metal (M) upon substrate (S). IHP and OHP indicates respectively, the inner and outer Helmholtz plane. The metal ions (M^{n+}) are surrounded by solvent molecules (w).*

Three main interactions can be considered in UPD processes:

(i)   deposit-electrode surface,

(ii)   anion-deposit,

(iii)   anion-electrode surface.

From these three interactions, the main driving force for the UPD process is generally the depositing metal-electrode surface interaction. However, the other two interactions can also play

important roles. The presence of strongly adsorbing anions in the electrolyte has particular importance, since the anion-metal and anion-substrate interactions can significantly modify UPD processes[37, 39, 47, 49, 76-80]. Anions, such as chloride, have been shown to form stable bilayers on electrode surfaces where the metal adatom is generally sandwiched between the electrode surface below and the anion adlayer above. In these cases, the strong interaction between the metal and the anion plays an essential role in bilayer formation.

 Early UPD studies were carried out mostly on polycrystalline electrode surfaces. This was due, at least in part, to the difficulty of preparing and maintaining single-crystal electrodes under well defined (and controlled) conditions of surface structure and cleanliness.

The advent of in-situ techniques eliminated much of the uncertainties involved and, as a result, generated great deal of interest. Especially, when coupled to studies on single-crystal surfaces, the techniques offered the opportunity for qualified characterizations. Of particular importance were the application of spectroscopic techniques such as FT-IR, Raman, and second harmonic generation (SHG). The development of *in situ* structural techniques based on either X-ray based methods (such as grazing incidence X-ray scattering, surface SEXAFS, and X-ray standing waves, among others) or scanned probe microcopies (STM, AFM, and related methods) further enhanced the ability to examine surfaces and surface structure at unprecedented levels of detail.

### 2.4.1 Theoretical Considerations for UPD

Underpotential deposition (UPD) of a metal (Me) onto a substrate (S) is due to a strong Me-S interaction and represents the initial step of metal crystallization. The formation of 2D Me_{ads} phases on S, in the underpotential range can be well described considering the substrate-electrolyte interface as an ideally polarizable electrode. The electrochemical double layer at the interface can be thermodynamically considered as a separate interphase. This interphase comprises region of the substrate and of the electrolyte with gradients of intensive system parameters such as chemical potential of ions and electrons, electric potentials, etc., and contains all adsorbates and all surface energies. Furthermore, it is assumed that the chemical potential $\mu_{Me_{ads}}$ is a definite function of the Me_{ads} surface concentration, Γ, and the electric potential, E, at constant temperature and pressure: $\mu_{Me_{ads}} = \mu_{Me_{ads}}\left(\Gamma,E\right)$. Such model system can only be realized

within a restricted potential range using inert noble metals (Au, Pt, Ag, etc.) as foreign substrates in contact with electrolytes containing solvated Me^{z+} ions.

The formation of Me$_{ads}$ on S corresponds to a transfer of solvated Me_{solv}^{z+} ions from the electrolyte phase (EI) to the interphase (IP) forming specifically adsorbed metal adions, Me_{ads}^{z+}, which are partially desolvated and located in the inner part of the electrochemical double layer:

$$Me_{solv}^{z+}(EI) \leftrightarrow Me_{ads}^{z+}(IP) \tag{Eq. 2.2}$$
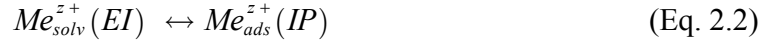
Simultaneously, the adsorbed species, $Me_{ads}^{z+}(IP)$ can interact with electrons of the interphase which can lead to a partial or complete discharge of $Me_{ads}^{z+}(IP)$:

$$Me_{ads}^{z+}(IP) + \lambda ze^-(IP) \leftrightarrow Me_{ads}^{z(1-\lambda)+}(IP) \quad with \quad 0 \leq \lambda \leq 1 \tag{Eq. 2.3}$$
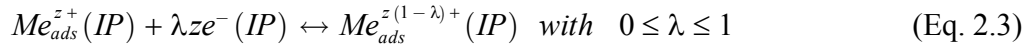
where λ is defined as the partial charge transfer coefficient. The partial charge number, $z(1-\lambda)$, of Me$_{ads}$ depends on the character of the adatom-substrate bond: λ is zero for a completely ionic bond and approaches 1 for a covalent bond where the Me-Me is the limiting case.

In the case of Me phase formation on foreign substrate S (λ=1), the overall reaction of the S/Me^{z+} electrode can be expressed in such a way:

$$Me_{(on\ top\ of\ S)} \Leftrightarrow Me_{solv}^{z+} + ze^- \tag{Eq. 2.4}$$

For 3D Me bulk phase on top of S, the thermodynamic equilibrium is given by the Nernst equation:

$$E_{Me/Me^{z+}} = E^0_{Me/Me^{z+}} + \frac{RT}{zF} \ln \frac{a_{Me^{z+}}}{a_{Me}} \tag{Eq. 2.5}$$

The actual electrode potential, *E*, determines the direction of reaction (2.4). This statement is valid , however, for 3D Me bulk phases only, while small 3D Me cluster phases have a more negative potential of stability, $E < E_{Me/Me^{z+}}$, $\Delta\mu > 0$ (supersaturation), and overpotential deposition (OPD) takes place . Under certain conditions, 2D Me phases are stable at $E > E_{Me/Me^{z+}}$ (underpotential deposition (UPD)) and $\Delta\mu < 0$ (undersaturation) on foreign substrate S. Therefore, the potential difference $E - E_{Me/Me^{z+}}$ is defined by convention as:

$$\Delta E\left(underpotential\right) > 0 \quad for \quad E > E_{Me/Me^{z+}}$$

$$E - E_{Me/Me^{z+}} \overset{def}{=}$$

$$\eta \left(overpotential\right) < 0 \quad for \quad E < E_{Me/Me^{z+}} \quad\quad (Eq.2.6)$$

The Nernst equilibrium potential, $E_{Me/Me^{z+}}$, represents the limit of the stability ranges of both 2D and 3D Me phases. At $E = E_{Me/Me^{z+}}$, 2D and 3D Me phases coexist. Consequently, underpotential deposition (UPD) and overpotential deposition (OPD) of Me on S are connected with the formation of 2D and 3D Me species, respectively.

The process of Me OPD on S becomes identical with that of Me OPD on Me if the deposited Me film on S exceeds a cartain thickness and behaves like a 3D Me bulk phase. Usually, the critical thickness varies between one and about twenty Me monolayers on S.

2.4.1.a Underpotential shift

Underpotentially deposited phases are more stable than the bulk phase of the adsorbate. A measure of this relative stability is given by the so-called underpotential shift $\Delta\phi_{upd}$ originally defined by Kolb et al. (eq. 2.7).

$$\Delta\phi_{upd} = \frac{1}{ze}\left(\mu\left[(M)M\right] - \mu\left[(S)M_\theta\right]\right) \quad\quad (Eq. 2.7)$$

where $\mu[(M)M]$ is the chemical potential of the adsorbate in the bulk phase and $\mu[(S)M]$ is the chemical potential of the adsorbate adsorbed at the substrate S at a coverage degree θ. The underpotential shift is available from experiment as the potential difference between the adsorption and bulk deposition peaks in a cyclic voltammogram.

2.4.1.b Work Function

Work function is a fundamental parameter in solid state science describing the electrochemical potential of the electrons in the electrode. It is directly related to the Fermi energy of a solid. In other definition, work function is the minimum energy (usually measured in electron volts) needed to remove an electron from a solid to a point immediately outside the solid

surface. Here "immediately" means that the final electron position is far from the surface on the atomic scale but still close to the solid on the macroscopic scale.

Changing the electrode potential by, say, 1 V in positive (negative) direction simply means a change of the Fermi level of the electrode by 1 eV to higher (lower) work function values. Indeed, the close correlation between PZC and work function for single-crystal metal surfaces has been demonstrated in various experiments [81]. Since the solvated ions, which provide the excess charge, have no chemical interaction with the electrode surface, the electrochemical work function of an electrode can be changed over a wide range without changing the chemical nature of the surface.

2.5 The Kinetics of the Formation of a Monolayer:

2.5.1 Nucleation and Growth mechanism & Avrami Analysis

Nucleation and growth behaviour as a consequence of a two dimensional phase transition is widely distributed in electrochemical systems, accompanied by faradaic reactions like in the different UPD systems [82, 83] or by only capacitive processes like in organic monolayers [14, 84-86].

The nucleation rate per surface unit can be calculated using the atomistic approach [87, 88] or the classical nucleation theory [89, 90]. The first is appropriate if a critical nucleous contains only a few atoms or molecules. The treatment of the nucleation rate according to the classical nucleation theory can be applied with reasonable precision, if the number of species in a critical nucleus is more than 15.

Nucleation and growth are the essentials of the kinetics of first-order phase transitions, which occur always in the metastable region in the Frumkin isotherm illustrated in Fig. 2.6 [91].
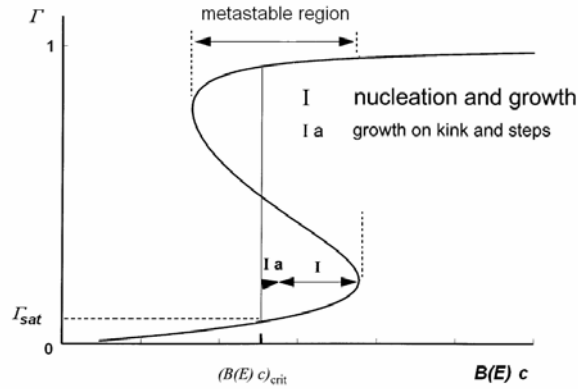
***Figure 2.6:** Schematic representation of the Frumkin isotherm. Concentrations of adsorbed species (B(E) c) depending on the considered potential regions versus surface coverage (Γ). Within the metastable region signed by vertical dotted lines nucleation and growth occur* [92].

***Nucleation** (hetereogenous):* if a reaction is not purely diffusion controlled, nucleation will play a significant role. Generally, nucleation rate, *J*, can be represented with the help of the following equations:

$$N(t) = N_0 \left[1 - \exp(-J't) \right] \qquad \text{(Eq. 2.8)}$$

$$J(t) = \frac{\partial N(t)}{\partial t} = N_0 J' \exp(-J't) \qquad \text{(Eq. 2.9)}$$

where *J'* is the steady state nucleation rate per active site. *N* is the number of nuclei. N_0 is the maximum possible number of nuclei in the absence of subsequent growth growth process. Two limiting cases of the exponential law of nucleation are of particular importance:

(i)   *J' >>* 1 :   *instantaneous nucleation*

$N(t) = N_0$ e.g. within the time all latently active centres are transformed into real nuclei at the very beginning of the condensation process.

(ii)   *J' <<* 1 :   *progressive nucleation*

$N(t) = J'N_0 t$ e.g. where the number of critical nuclei increases linearly with time.

The steady state rate of 2D nucleation is strongly dependent on the dimensionality of the active sites. Staikov et al. reported that, at constant supersaturation, *J*(terrace) < *J*(step) < *J*(kink) [84, 93]. Active sites represent not only surface imperfections, but may be also generated by surface oxidation/reduction, reconstruction processes or ad/desorption of anions or solvent molecules [94].

The combination of active intermediates to form a critical nucleus at a specific site may lead to the power law of n–step nucleation;

$$N(t) = J'' N_0 t^n$$
<div align="right">Eq. 2.10</div>

J′′ represents the modified nucleation rate [95].

Growth: The expansion of a supercritical nucleus through continued incorporation of monomers is called growth. If the resulting new phase is isotropic, as for instance in the case of a circular island, a single, time-independent growth rate, k_G, is enough to characterize the process. For anisotropic growth, there will be several growth rates [84]. For 2D growth, expansion of the clusters is possible only at its periphery. Referring to the elementary process involved on an ideally smooth surface, one may distinguish two main mechanisms:

(i) growth controlled by the *rate of monomer incorporation*

(ii) *mass transport* (surface diffusion)-controlled growth [96].

Assuming that the incorporation is the rate – determining step (i), the growth rate, *G(t)*, the number of condensed monomers, *$N_c(t)$,* belonging to an isolated circular cluster of height *h* obeys the equation:

$$G(t) = \frac{\partial N_c(t)}{\partial t} = 2\pi k_G r(t) h$$
<div align="right">(Eq. 2.11)</div>

$$\text{with} \quad r(t) = \left(k_G / \rho \right) t$$
<div align="right">(Eq. 2.12)</div>

ρ is the number of particles per unit area. Normalization to the real surface area, S_E, and to the maximum surface excess of the condensed phase, Γ_m, yields the fractional coverage of this phase as

$$\frac{\partial \theta}{\partial t} = \frac{2\pi h\, k_G^2\, M}{\rho S_E \Gamma_m}\ t = K_1\, t = f_1(t)$$
<div align="right">(Eq. 2.13)</div>

If the rate of advance of the growing circular centre is controlled by symmetrical hemicylindrical (surface) diffusion (ii) about an axis perpendicular to the 2D nucleus one obtains

$$r(t) = A\sqrt{Dt}$$
<div align="right">Eq. 2.14</div>

where A is a constant depending on potential, molecular weight and density of the monomer, and D is the diffusion coefficient [97]. The corresponding coverage function is given by

$$\frac{\partial \theta}{\partial t} = \frac{2\pi h A^2 D\rho}{MS_E \Gamma_m} = K_1^{'}$$

<div align="right">Eq. 2.15</div>

Coupling of nucleation and growth

The rate of nucleation *J(t)* and the growth rate *G(t)* are both function of the applied supersaturation (e.g. electrode potential [84] or difference in surface energy [98], respectively). Three basic regimes may be distinguished: If the formation period of the critical cluster is much longer than the time required covering the available electrode surface by its subsequent growth, the transformation involves just one nucleus, and is called *mononucleation*. If the rate of nucleation is much faster than the subsequent growth process, many nuclei contribute to the creation of the new phase. This regime is known as *polynucleation*. The intermediate case, which involves just a few nuclei, is named *oligonucleation*.

Mononucleation events at electrochemical interfaces have been observed in potential step experiments by monitoring current, charge or capacitance as a function of time under conditions of (i) low supersaturation and (ii) small, defect-free electrode surfaces. These experiments offer the unique opportunity to determine simultaneously absolute rates of the nucleation and growth processes.

At high supersaturation many nuclei are created independently (*polynucleation*). The completion of the transition proceeds by subsequent growth of a large number of nuclei. In the initial stages of formation of the new phase, the individual centres can be assumed to grow rather independently of each other. The extended fractional coverage, θ_{ext}, e.g. the hypothetical coverage representing the unhindered growth of individual nuclei, is obtained by solving the following convolution integral [22, 96]

$$\theta_{ext} = \int_0^t \left(\frac{dN}{dt}\right)_{t=z} \delta\left(\int_z^t G(u)du\right)^2 dz$$

<div align="right">(Eq. 2.16)</div>

with θ_{ext} = extended surface coverage of all islands (here "extended" means that the possible overlap of growing islands is not accounted for), dN/dt = rate of nucleation ($J(t)$), $G(t)$ = rate of radial growth, and δ = form factor (e.g. π for cylindrical islands).

The extended coverage, θ_{ext}, and the „true" coverage θ, as obtained in reality by internuclear collision and overlap of the growing centers at an advanced stage of the transition, are related within the framework of the Avrami-theorem [99, 100].

It was first shown in two classical papers by Avrami [99, 100] (see Fig. 2.6) that the coverage, θ, is related to θ_{ext} by

$$\Theta = 1 - \exp(-\theta_{ext}) \qquad\qquad \text{(Eq. 2.17)}$$

As θ_{ext} becomes very large, Θ tends toward 1; that is, the surface is completely covered. The charge density associated with this extended area is given by the centers cannot grow freely in all directions, since they will impinge on each other. For the formation of solid phases, growth must stop at the points of contact. The problem has been treated theoretically by introducing the notion of the *extended coverage, θ_{ext},* defined as the area which would be covered by the centers if the overlap were not occurring.
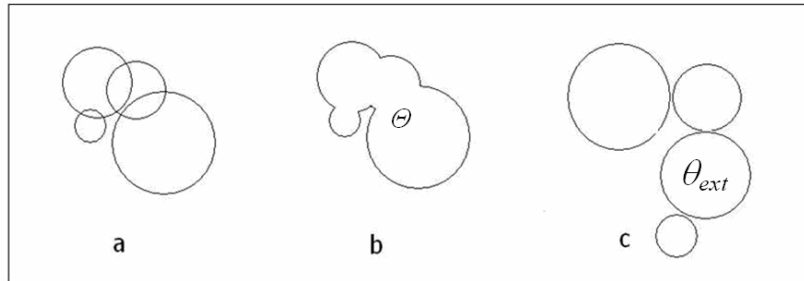
Figure 2.6: *The overlap problem. The Avrami theorem relates the true surface coverage, Θ, to the extended coverage, θ_{ext}. The figure illustrates how the overlap of growth centers shown in (a) gives rise to the real coverage corresponding to (b) and the "extended coverage" shown in (c).*

The combination of Eq. 2.16 and 2.17 with the exponential law of nucleation (Eq. 2.9), and growth of circular 2D clusters by direct *incorporation* of monomers (constant growth) (Eq. 2.13) yields the following equations at the limiting cases;

$$\Theta = 1 - \exp\left(-2K_1 N_0 J' t^2\right) \qquad \text{for} \quad J' \to \infty \qquad \text{(instantaneous nucl.)} \qquad \text{(Eq. 2.18.a)}$$

$$\Theta = 1 - \exp\left[-\frac{2K_1 N_0 J'}{3} t^3\right] \qquad \text{for} \quad J' \to 0 \qquad \text{(progressive nucl.)} \qquad \text{(Eq. 2.18.b)}$$

The combination of Eq. 2.16 and 2.17 with the exponential law of nucleation (Eq. 2.9), and *surface diffusion* controlled growth (Eq. 2.15) yields the following equations at the limiting cases;

$$\Theta = 1 - \exp\left(-2K'_1 J' N_0 t\right) \qquad \text{for} \quad J' \to \infty \qquad \text{(instantaneous nucl.)} \qquad \text{(Eq. 2.19.a)}$$

$$\Theta = 1 - \exp\left(-K'_1 N_0 J' t^2\right) \qquad \text{for} \quad J' \to 0 \qquad \text{(progressive nucl.)} \qquad \text{(Eq. 2.19.b)}$$

The above expressions of polynucleation and growth processes, as triggered by single potential step experiments $E_1 \to E_2$, may be represented by the general Avrami–equation [21, 30]

$$\Theta = 1 - \exp\left(-Kt^m\right) \qquad\qquad \text{(Eq. 2.20)}$$

$$\boxed{\ln\left[\ln\left(\frac{1}{1-\Theta}\right)\right] = m \ln t + \ln K} \qquad\qquad \text{(Eq. 2.21)}$$

K is a constant; Θ stands for the surface coverage of the condensed phase, m is related with the sum of the dimension and time exponent in the nucleation law.

The Avrami theorem Avrami equation (Eq. (2.21)) is generally valid and independent of the models describing the coupling of nucleation and growth behaviour. Commonly, the slope m serves as a diagnostic criterion to determine the nucleation and growth mechanism [91, 95].

The combination of the limiting cases of progressive and instantaneous nucleation together with the limiting cases for the growth laws are summarized in Table 2.1. They can be classified as *constant* or *surface diffusion* controlled growth laws, having characteristic integer slopes of the Avrami plot. It should be emphasized that an integer value generally denotes a linear Avrami plot and is therefore explicitly defined. In contrast, a non-integer value indicates the validity of the general exponential law of nucleation itself, in combination with both limiting cases of growth behaviour. Slopes between 2 and 3 indicate constant growth, whereas slopes between 1 and 2 indicate surface diffusion growth.

Avrami slope (*m*)	Nucleation Mechanism	Growth Mechanism
1	*Instantaneous*	Surface diffusion
1 < *m* < 2	Exponential law	Surface diffusion
2	*Instantaneous* / <u>progressive</u>	*Constant* / <u>surface diffusion</u>
2 < *m* < 3	Exponential law	*Constant*
3	Progressive	*Constant*
m > 3	Power law	*Constant* / surface diffusion

Table 2.1*: Avrami slopes as diagnostic criteria for the nucleation and growth mechanism* [95].

A comparison between the Avrami slopes *m* obtained from conventional concepts and from the more general physicochemical approach considering the coupling of adsorption and condensation opens up new possibilities for a more detailed analysis of experimental data. It should be pointed out that Eq. 2.21 represents only one kind of illustration of surface-coverage-time curves. In our studies we choose this kind of data presentation, because the deviation of the Avrami plots from linearity indicates in an illustrative way the influence of the time dependent supersaturation.

2.5.2 Dissolution kinetics interpreted by the predator-prey model: *Coupling of dissolution and desorption*

The predator-prey model describes the first order phase transition as a coupling of adsorption and the real condensation process [101]. The first model, which discusses explicitly this way of coupling of adsorption and condensation, was developed by Markov [102]. In order to model the kinetics, one must consider two consecutive steps to get information on the *supersaturation* as the driving force of the process, the adsorption of the species onto the electrode surface followed by the two dimensional nucleation and growth (Fig. 2.7.a).

The model can also be applied for the description of the dissolution kinetics. In the present case, the mechanism is a *hole* nucleation and growth process. The driving force is the *undersaturation* and the two consecutive steps comprise the *dissolution* of the condensed phase followed by the *desorption* of the species from the electrode surface (Fig. 2.7.b). The kinetics can be described only by a coupled system of four coupled differential equations. The derivation of

all equations are presented by Donner [91]. Those equations describe the time dependencies of the driving force, the surface coverage of the phase, the length of the periphery of the phase and the number of formed nuclei. This equation system can be solved only numerically, whereby the fitting procedure is a time consuming process, because the equation system depends on four independent constants.
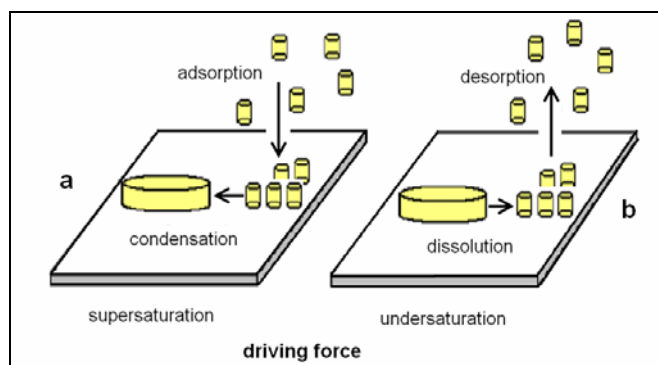
Figure 2.7: *Sketches representing the Predator-prey model for supersaturation (a) and undersaturation (b) to determine the overall kinetics of a 2D first order phase transition.*

In case that one process (adsorption/desorption or condensation/dissolution) is accompanied by a faradaic electron transfer, much more charge flows during this process than in the other processes, which are of capacitive nature. So they can be neglected in a first approximation. For such an ideal system an Avrami check yields information on the time-dependence of the driving force and the nucleation mechanism according to [91, 92].

In our system, we will describe only the dissolution process as a nucleation and growth process. The electrode surface at time t can be considered as a parallel assembly of three capacitors corresponding to the free electrode surface (in our case the thymine covered Au(111) surface), the surface covered by copper adatoms and by an ordered copper and/or thymine layer (UPD layer). The charge q at time t obeys the equation:

$$q = (1-\Theta)q_{\text{free-surface}} + \Theta q_{\text{upd}} \qquad \text{(Eq. 2.22)}$$

Θ: ratio between the areas covered by the UPD layer (condensed layer) to the whole electrode area,

q_{upd} : charge of area covered by the UPD layer

$q_{\text{free-surface}}$: charge of the free surface

At the free surface (1 − Θ), copper adatoms (with thymine) are adsorbed:

$$q_{\text{free-surface}} = (1 − \Gamma)q_{\text{elect.}} + \Gamma q_{\text{adatom}} \qquad \text{(Eq. 2.23)}$$

Γ: ratio of the of the actual copper adatom concentration to the maximum concentration,

$q_{\text{elect.}}$: charge of the area covered by the electrolyte and the thymine molecules,

q_{adatom}: charge of the area covered by copper adatoms.

Differentiation of Eq. 2.22 after time leads to the well known equation for the current flowing during the whole dissolution process:

$$I(t) = \Delta q_1 (1 − \Theta)\frac{d\Gamma}{dt} + \Delta q_2 \frac{d\Theta}{dt} \qquad \text{(Eq. 2.24)}$$

Δq_1: charge difference between the surface covered by copper adatoms and the free surface,

Δq_2: charge difference between the surface covered by the UPD layer (condensed layer) and the surface covered by copper adatoms.

The current (Eq. 2.24) consists of two contributions, one is for the true dissolution and the second one is for the desorption of copper species. In principle, one can distinguish between the two cases:

i)   The metal adatoms are discharged at that time at which they lose their contact with the electrode surface. This is the equivalent situation as it was described for nonfaradaic phase transitions [91].

ii)   The metal adatoms are discharged at that time at which they leave the UPD layer. This assumption seems more reasonable than the former one. Capacitive parts can be neglected due to the desorption of metal adatoms and/or the reorientation of organic molecules such as thymine.

Considering the ideal case (ii), the dissolution transients can be analysed to investigate the time dependence of hole nucleation and growth mechanism using Avrami plots as was discussed in [91]. The lower the undersaturation is, the higher is the driving force for the dissolution or the lower driving force for the desorption. The Avrami slopes increase with decreasing undersaturation. In contrast, the increasing concentration of the copper adatoms leads to a

decrease of the driving force for dissolution, the hole nucleation rate as well as the Avrami slopes decrease.

By this simple Avrami test we cannot distinguish between the different nucleation mechanisms but we can define the time dependent *ratio* of the dissolution to the desorption kinetics.

In our experiments, we have investigated the nucleation and growth mechanism for the deposition and dissolution of metal or metal/organic adlayers considering commonly used Avrami plots. For the sake of simplicity, we restrict our considerations to two parts; the first is the usability of the conventional concepts of progressive and instantaneous nucleation (Table 2.1), the second is the application of the predator-prey model [91, 92, 101] to our system in the frame of time-dependent supersaturation/undersaturation.